Lab on a Chip

# In-droplet cell separation based on bipolar dielectrophoretic response to facilitate cellular droplet assays



| | |
|---|---|
| Journal: | *Lab on a Chip* |
| Manuscript ID | LC-ART-07-2020-000710.R2 |
| Article Type: | Paper |
| Date Submitted by the Author: | 28-Aug-2020 |
| Complete List of Authors: | Han, Song-I; Texas A&M University College Station, Electrical and Computer Engineering<br>Huang, Can; Texas A&M University College Station, Electrical and Computer Engineering<br>Han, Arum; Texas A&M University College Station, Electrical and Computer Engineering |
| | |

ARTICLE

# In-droplet cell separation based on bipolar dielectrophoretic response to facilitate cellular droplet assays

Received 00th January 20xx,
Accepted 00th January 20xx

DOI: 10.1039/x0xx00000x

Song-I Han,[†a] Can Huang,[†a] and Arum Han*[ab]

Precise manipulation of cells within water-in-oil emulsion droplets has the potential to vastly expand the type of cellular assays that can be conducted in droplet-based microfluidic systems. However, achieving such manipulation remains challenging. Here, we present an in-droplet label-free cell separation technology by utilizing different dielectrophoretic responses of two different cell types. Two pairs of angled planar electrodes were utilized to generate positive or negative dielectrophoretic force acting on each cell type, which results in selective in-droplet movement of only one specific cell type at a time. A downstream asymmetric Y-shaped microfluidic junction splits the mother droplet into two daughter droplets, each of which contains only one cell type. The capability of this platform was successfully demonstrated by conducting in-droplet separation from a mixture of *Salmonella* cells and macrophages, two cell types commonly used as a bacterial pathogenicity infection model. This technology can enable the precise manipulation of cells within droplets, which can be exploited as a critical function in implementing broader ranges of droplet microfluidics-based cellular assays.

## Introduction

In recent years, water-in-oil emulsion droplet-based microfluidics systems have demonstrated great potentials for broad ranges of biological assays and investigations. Due to its capability of handling extremely small volume of biological samples and liquid at very high-throughput, droplet-based microfluidics technology has become an ideal and powerful tool in facilitating cellular studies, and so far has been well established and widely utilized in high-throughput, single cell resolution assays, aiming to substitute time-consuming and labor-intensive conventional biotechnology laboratory methods.[1-4] Up until now, in order to transfer the conventional laboratory sample handling practices into a droplet microfluidics format, many different droplet microfluidics functions have been realized, such as cell encapsulation technology for creating isolated nano/pico-liter-scale bioreactors, droplet merging technology for mixing samples and reagents, droplet detection and sorting technology for analyzing assay results and retrieving samples.

Despite the fact that most liquid-handling technologies are now readily available in droplet microfluidics format, it still remains challenging to achieve in-droplet cell separation. There are many different applications that can benefit from in-droplet cell separation capabilities, of which one large application area being studying cellular interaction. For example, in broad ranges of microbiological studies, cellular interaction is one of the key topic area for obtaining insights into cellular mechanisms that drive cell-cell communication,[5] pathogenicity based on host-pathogen interaction,[6-8] immune responses,[9] to name a few. In conventional bulk-scale cellular interaction studies, different types of cells of interest are typically first mixed together and co-cultured for a certain period of time to allow the occurrence of cell-cell interactions, followed by analyzing the result and then ideally separating out the different cell types for further downstream investigation. Many researchers have successfully developed continuous-flow-based microfluidics platforms to achieve microfluidic pathogenicity studies, covering applications in studying cell-cell interactions, cytoadhesion, cytotoxicity, and immunological responses.[10-14] Performing these types of assays in droplet microfluidics platforms is highly desired, especially when large number of diverse heterogeneous cell samples have to be screened and tested, such as screening environmental or synthetic microbial libraries. For example, in host-pathogen adherence assay, in order to determine the degree of pathogenicity caused by microorganisms, bacterial cells are co-incubated with host cells, then free-floating bacterial cells are rinsed off to recover only microbes that adhere to the host cells.[15-17] Failure of effectively separating bacterial cells from host cells will lead to high false-positive rates as the degree of attachment will be misread when non-adherent microbes are remained during post analysis. Another example that requires in-droplet cell separation could be in drug screening applications, where in-droplet cell separation can lead to obtaining only pure cell samples of interest.

[a] Department of Electrical and Computer Engineering, Department of Biomedical Engineering, Texas A&M University, College Station, TX 77843, USA
[b] Department of Biomedical Engineering, Texas A&M University, College Station, TX 77843, USA, E-mail: arum.han@ece.tamu.edu
† These authors contributed equally to this work.
Electronic Supplementary Information (ESI) available: [details of any supplementary information available should be included here]. See DOI: 10.1039/x0xx00000x

Overall, in the context of droplet microfluidics systems, in-droplet content manipulation technologies developed so far have been challenging to achieve selective cell separation and/or targeted content removal from within droplets. Thus, in -droplet cell separation techniques have the potential to further widen the bandwidth of droplet-based microfluidic technologies and extent broader ranges of cellular assays to be implemented in such format.

Several studies have been reported aiming to enable such in-droplet content manipulation technology. Aside from some passive methods,[18-20] active methods of in-droplet particle/cell manipulation require external force to be applied but can also achieve more precise manipulation. Several active manipulation methods have been realized by using magnetic beads,[21-23] acoustophoresis,[24-29] and dielectrophoresis (DEP).[30] Magnetic bead-based manipulation was exploited for target molecule separation such as human serum albumin,[21] mRNA,[22] and prostate-specific antigens in droplets to achieve drug analysis,[23] molecular detection, and immunoassays. However, since labelling step is essential in this method, this cannot be used when tagging cannot be performed at the beginning of the assay, or when the downstream assay is not compatible with magnetic beads. In addition, this extra labelling step limits its compatibility and makes it cumbersome to be implemented.

Acoustophoresis, a label-free particle/cell manipulation technique, has been used for in-droplet particle or cell manipulation. Fornell et al.[24-26] have demonstrated that particles and cells can be focused to the center of a droplet or to both sides of a droplet using first or second harmonic standing acoustic wave generated by bulk acoustic wave (BAW) due to their intrinsic positive acoustic contrast factor compared to carrying media. As all particles or all cells were moved to a particular location within the droplet, in-droplet particle/cell concentration was achieved with relatively high throughput (4 droplets $s^{-1}$) and high focusing efficiency (90%). In a follow-up study, they have further developed this into in-droplet particle separation based on different acoustic contrast factors (polystyrene vs polydimethyl siloxane (PDMS) particles).[27] However, this technology is somewhat limited when separating two different population of cells. Since all cells suspended in regular culture media have positive acoustic contrast factors, applying acoustic manipulation will result in all cells to move towards the same position within a droplet. Thus, these approaches are not suitable for selective manipulation of cells of interest from a cell mixture. Additionally, BAW device fabrication requires the use of hard materials, such as glass or silicon, to achieve acoustic wave propagation with low attenuation. An alternative approach in acoustophoresis is the use of surface acoustic wave (SAW). Park et al. have demonstrated in-droplet particle separation using travelling SAW based on different acoustic radiation force factors depending on the particle size.[28] Additionally, they have further demonstrated in-droplet particle washing by handling both droplets and particles using SAW, simultaneously.[29] However, so far SAW-based in-droplet separation has not been demonstrated with real biological samples such as cells. Thus, the feasibility of separating cells based on their different acoustic properties within droplets remains untested.

Dielectrophoresis (DEP) is an electrical field-based label-free cell manipulation method, which can be readily integrated in a microfluidic format, since only a simple patterned electrode placed on the bottom of a microfluidic channel is needed. Thus, DEP microfluidic technologies have been extensively used in particle and cell manipulation in free-flow microfluidics.[31-34] In DEP-based manipulation, cell experiences positive DEP force (pDEP, i.e., attracted to the electrode), negative DEP force (nDEP, i.e., repelled away from the electrode), or neutral response, depending on the frequency applied as well as the dielectric properties of cells and their surrounding media. Previously, we have successfully

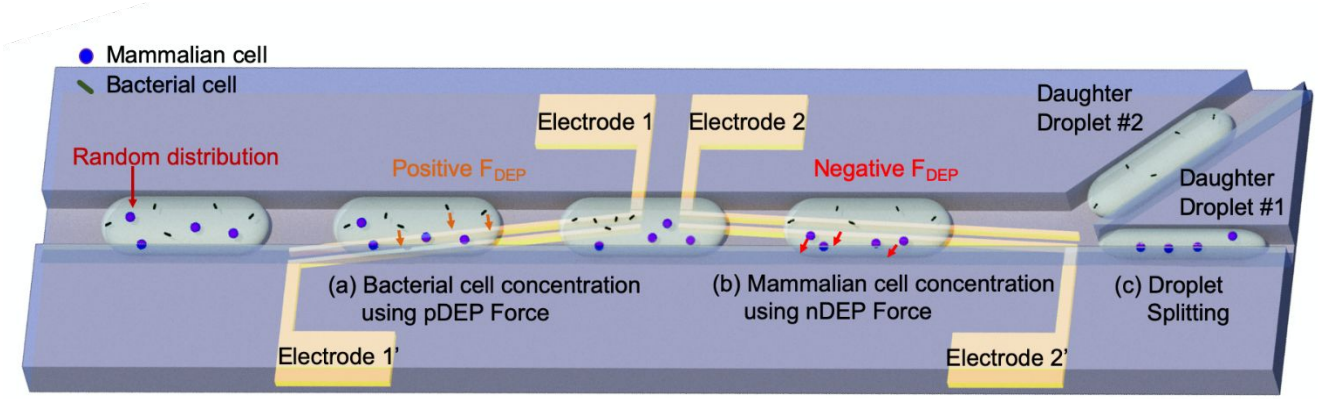


**Fig. 1** Schematic illustration of the in-droplet cell separation platform composed of: (a) A first DEP electrode pair that tilts upwards for bacterial cell manipulation using pDEP force, resulting in accumulation of all bacterial cells to the upper part of the droplet; (b) A second downward-tilted DEP electrode pair for mammalian cell manipulation using nDEP force, resulting in concentration of all mammalian cells to the lower half of the droplet, while bacterial cells are unaffected and thus remain circulating within the upper half of the droplet by the internal circulation flow; (c) An asymmetric droplet splitter that divides the mother droplet into two daughter droplets, the upper split droplet (daughter droplet #1) containing only bacterial cells and the lower split droplet (daughter droplet #2) containing only mammalian cells.

demonstrated in-droplet particle and cell manipulation using nDEP, where particles/cells could be accumulated to one side of the droplets and thus enriched into one of the daughter droplets.[30] However, in this case, all cells, regardless of the cell types, were concentrated towards the same side of the droplet. Therefore, this design could not be used to specifically manipulate a target cell population from mixing sample, thus in-droplet cell separation based on the cellular properties was not feasible under such setting.

In this paper, we exploited, for the first time, the differences in DEP responses of different cell types under specific frequencies to achieve precise in-droplet cell separation of two different populations. Here, two sequential DEP electrode arrays were utilized so that one cell type experiences pDEP force and another cell type experiences nDEP force, resulting in the two different cell types to be moved to opposite sides within a given droplet. By splitting the droplet into two daughter droplets after the in-droplet DEP manipulation of cells, the different cell types could be separated into each of the two daughter droplets, respectively. Here, to better elucidate the capability as well as the applications of the proposed DEP-based in-droplet cell separation platform, mammalian host cells and bacterial cells were chosen to be used to mimic a common model system when studying host-pathogen interaction.

## Results

### Working principle

Two pairs of planar parallel DEP electrodes were used to generate a high-gradient non-uniform electric field at the edges of the electrodes. The time-averaged $x$-direction DEP force can be described by Equation 1.[35]

$$F_{dx} = 2\pi\varepsilon_m r^3{}_c Re[f_{CM}]\frac{\partial|\vec{E}|^2}{\partial x} \quad (1)$$

According to this equation, the DEP force here is determined by $\varepsilon_m$, the permittivity of the surrounding solution, $r$, the cell radius, $Re[f_{CM}]$ ($f_{CM} = \frac{\varepsilon_c^*(\omega) - \varepsilon_m^*(\omega)}{\varepsilon_c^*(\omega) + 2\varepsilon_m^*(\omega)}, \varepsilon^* = \varepsilon - j\frac{\sigma}{\omega}$), real part of the *Clausius-Mossotti* factor, and the applied voltage. Specifically, the DEP force is proportional to the real part of the *Clausius-Mossotti* factor, by which the magnitude of DEP force and DEP polarity are determined.

In this study, mammalian cells (J774A.1 macrophages) and bacterial cells (*Salmonella Typhimurium*) were used as a model system of bacterial cell – mammalian host cell interaction to demonstrate the feasibility of separating two different types of cells from a mixture depending on their different DEP responses inside a droplet. An in-droplet DEP cell separation system consists of a first DEP manipulation region for bacterial cells concentration (Fig. 1(a)), a second DEP manipulation region for mammalian cells concentration (Fig. 1(b)), and a droplet splitter (Fig. 1(c)). In front of the DEP separation units, a flow-focusing design droplet generator was placed to encapsulate bacterial cells and mammalian cells into a droplet (Fig. S1). Mammalian cell suspension and bacterial cell suspension were injected from two separate inlets, mixed at the first crossing, then went into the flow-focusing structure where droplets containing the cell mixture were generated. All generated droplets were flown through the DEP separation units having two sets of an angled DEP electrode pair placed at the bottom of a microfluidic channel.

Before reaching the DEP separation regions of the microfluidic channel, all cells in droplets have random

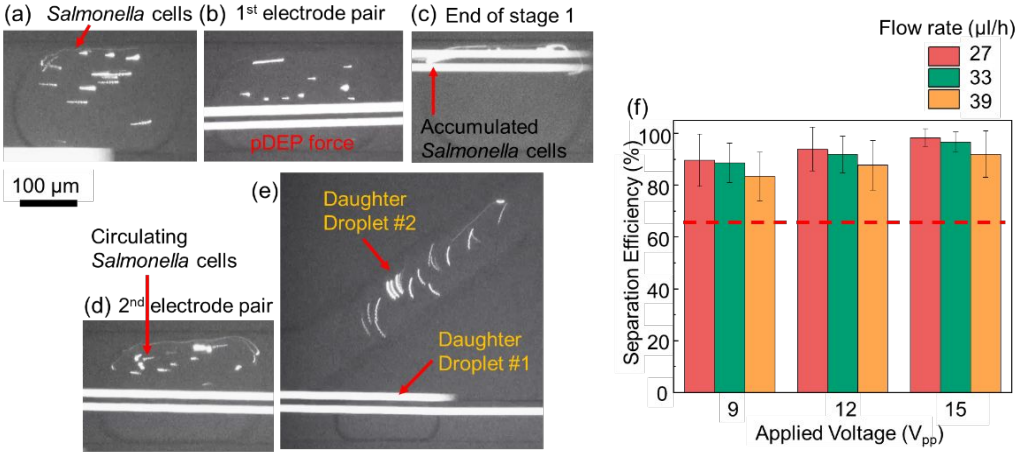


**Fig. 2** Movement of *Salmonella* cells within a droplet as the droplet travels through the electrodes. (a) A droplet containing 17 *Salmonella* cells was generated and randomly distributed within the droplet. (b-c) As the droplet passes through the first DEP electrode pair, *Salmonella* cells were attracted to the angled electrodes due to pDEP force once they were close to the electrode, accumulating at the upper half of the droplet. (d) Even though *Salmonella* cells were not affected by any DEP force while passing through the second DEP electrode pair, they remain within the upper half of the droplet by the internal circulation flow. (e) The droplet was split into two daughter droplets, with the upper daughter droplet containing all the *Salmonella* cells. (f) *Salmonella* cell separation efficiencies into daughter droplet #2 at different flow rates and voltages tested. Flow rates were set to be 27, 33 and 39 μl $h^{-1}$, each with three applied voltages varying from 9, 12, to 15 $V_{pp}$. At 27 μl $h^{-1}$ and 15 $V_{pp}$, the *Salmonella* cell separation efficiency reached 98%.

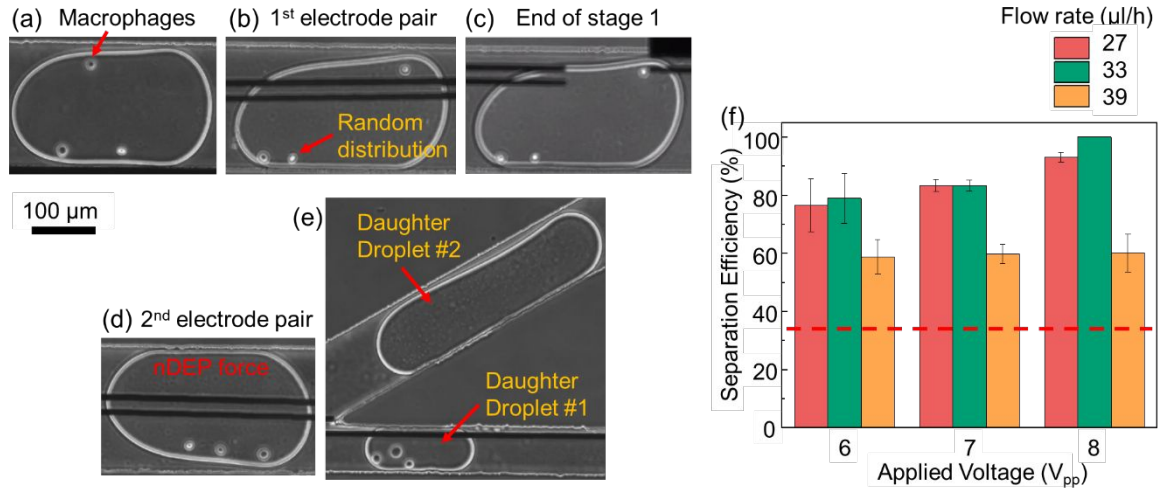


**Fig. 3** Movement of macrophages within a droplet as the droplet travels through the DEP electrodes. (a) A droplet containing three macrophages is shown, randomly distributed. (b-c) The macrophages are not affected by the DEP force and remain randomly distributed while passing through the first DEP electrode pair. (d) As the droplet passed through the second DEP electrode pair, macrophages were repelled away from the electrode edges, resulting in all macrophages to be pushed towards the lower side of the droplet. (e) The droplet was split into two daughter droplets, with the lower daughter droplet containing all three macrophages. (f) Macrophage separation efficiencies into daughter droplet #1 at different flow rates and voltages tested. Flow rate was set to be 27, 33 and 39 μl $h^{-1}$, each with three applied voltages varying from 6, 7, to 8 $V_{pp}$. At 33 μl $h^{-1}$ and 8 $V_{pp}$, the macrophage separation efficiency was 100%.

distribution. As the droplets pass through the first pair of DEP electrodes, the upward-tilted electrodes function as a guiding track as bacterial cells affected by pDEP force are attracted to the electrode gap. Based on this simulation result of the *Clausius-Mossotti* factor (Fig. S2), by choosing a frequency (6 MHz) where mammalian cells receive no DEP force, only bacterial cells are accumulated to the upper half of the droplet by pDEP force, while leaving the mammalian cells randomly distributed within the droplet (Fig. 1(a)). Then, as the droplets pass through the second pair of DEP electrodes, since the bacterial cells have been already accumulated to the upper half of the droplet, by choosing a frequency (100 kHz) where bacterial cells have no DEP response, the bacterial cells remain within the upper half of the droplet due to the internal circulation flow in each half of the droplet. Meanwhile, mammalian cells experience nDEP force and are pushed away from the downward-tilted electrodes, always staying below the electrodes and thus gradually accumulating to the lower part of the droplet (Fig. 1(b)). Once the droplet reaches the asymmetric droplet splitting region, the mother droplet is split into two daughter droplets, where bacterial cells that remain in the upper half splits into a bacterial cell-only droplet, while mammalian cells that remain in the lower part of the droplet splits into a mammalian cell-only droplet (Fig. 1(c)).

**Characterization of in-droplet bacterial cell manipulation**

Droplets containing only *Salmonella* cells were generated at a concentration of approximately 20 cells per droplet, and all *Salmonella* cells in the droplet show random distribution (Fig. 2(a)). The droplets flow through the DEP cell separation region of the platform at a flow rate of 33 μl $h^{-1}$. As the droplets containing *Salmonella* cells travel through the first pair of DEP electrodes (3 MHz, 15 V peak-to-peak ($V_{pp}$)), the *Salmonella* cells that came close to the tilted electrodes experienced pDEP force, resulting in attraction towards the electrodes (Fig. 2(b)). Since this electrode starts from the bottom side of the droplet, *Salmonella* cells circulating in the lower part of the droplet can be gradually moved to the upper part of the droplet by accumulating along the upward-tilted electrode. At the end of the first DEP electrode pair, all *Salmonella* cells were confined to the upper side of the droplet (Fig. 2(c)). As the droplet travelled through the second pair of DEP electrodes (100 kHz, 8 $V_{pp}$), the accumulated *Salmonella* cells were released from the electrodes since bacterial cells experience no DEP force at this frequency. However, the *Salmonella* cells remained circulating within the upper half of the droplet due to the internal circulation of flow within the upper half of the droplet (Fig. 2(d)). When reaching the droplet splitting region, these accumulated *Salmonella* cells were split into the daughter droplet #2 (Fig. 2(e)). Comparison of the daughter droplets collected in the downstream chambers shows the successful concentration of *Salmonella* cells into the upper chamber (Fig. S3(a)). In this analysis, *Salmonella* cells, separated into daughter droplet #1 and #2, respectively, were manually counted under GFP filter condition (ex/em 495/519 nm), and then used to calculate the separation efficiency.

Next, further device characterization was conducted under three different DEP voltages applied (9, 12 and 15 $V_{pp}$) and at three different flow rates (27 μl $h^{-1}$ = 1.2 droplets $s^{-1}$, 33 μl $h^{-1}$ = 1.5 droplets $s^{-1}$, and 39 μl $h^{-1}$ = 1.8 droplets $s^{-1}$) while keeping the droplet size the same. As expected, higher voltage and lower flow rate separate cells more efficiently, thus providing a

higher separation efficiency (Fig. 2(f)). The optimal operation condition was found to be at 27 μl $h^{-1}$ at 15 $V_{pp}$, and the maximum separation efficiency for *Salmonella* cells could reach 98 ± 3%. However, even at 33 μl $h^{-1}$, the separation efficiency was still relatively high (97 ± 4%), while the overall system throughput could be increased by 20%. The separation efficiency dropped to 92 ± 9% at 39 μl $h^{-1}$. Thus, considering the overall trade-off, the flow rate of 33 μl $h^{-1}$ and applied voltage of 15 $V_{pp}$ was selected to be the ideal condition (ESI video #1) for the remainder of the experiments.

**Characterization of in-droplet mammalian cell manipulation**

The number of macrophages encapsulated per droplet was around 4 as in most bacterial infection models the number of bacterial cells typically outnumber that of mammalian host cells. All conditions used here such as the DEP frequency and amplitude of voltage, as well as flow rate, were identical to those used for the in-droplet *Salmonella* cell manipulation characterization steps. Before the droplets reached the first pair of DEP electrodes, all macrophages were randomly distributed within the droplet (Fig. 3(a)). When passing through the first electrode pair, macrophages received no DEP force (Fig. 3(b)) and remain randomly distributed (Fig. 3(c)). As they pass through the second pair of DEP electrodes, macrophages experienced nDEP force and were repelled away from the electrode, therefore gradually confined below the electrode and into the lower half of the droplet (Fig. 3(d)). After droplet splitting, all macrophages were separated into the daughter droplet #1, while no macrophages were seen in the daughter droplet #2 (Fig. 3(e)). Comparison of the daughter droplets collected in the downstream chambers shows the successful concentration of macrophages into the lower chamber (Fig. S3(d)). The separation efficiency was analyzed using bright filed microscopy images.

Further device characterization was conducted under three different DEP voltages (6, 7 and 8 $V_{pp}$) and three different flow rates (total flow rate: 27, 33, and 39 μl $h^{-1}$). In the case of macrophages (Fig. 3(f)), the overall separation efficiency increased as the flow rate decreased or when the applied voltage increased. Even though the separation efficiency at the flow rate of 33 μl $h^{-1}$ was somewhat higher than that at 27 μl $h^{-1}$, the separation efficiency with standard deviation was comparable to each other under the same applied voltage condition. When 8 $V_{pp}$ was applied, the separation efficiencies at flow rates of 27 and 33 μl $h^{-1}$ were 93 ± 8% and 100%, respectively, demonstrating very efficient macrophage manipulation. However, a higher flow rate (39 μl $h^{-1}$) caused increase of the internal circulation flow force, thus the separation efficiency was about 60 ± 7% among all voltage conditions tested, indicating that an even stronger DEP voltage is required to achieve sufficient force for in-droplet cell manipulation. Overall, by varying the voltage as well as the flow rate, an optimal condition was found to be at an applied voltage of 8 $V_{pp}$ and at a flow rate of 33 μl $h^{-1}$ (ESI video #2).

**In-droplet cell separation**

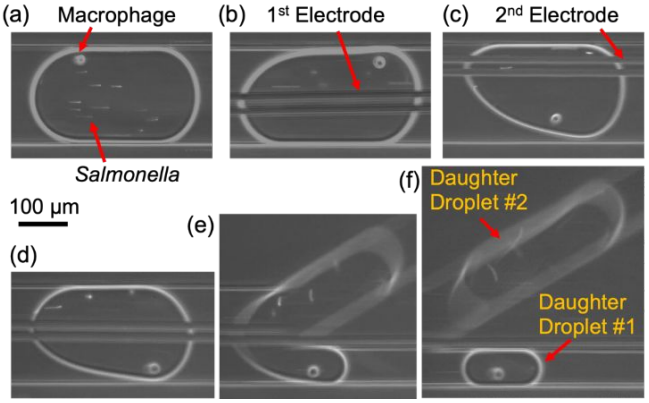


**Fig. 4** Movement of *Salmonella* cells and a macrophage inside a droplet. The operation conditions were set to 100 kHz, 8 $V_{pp}$ at the first DEP electrode pair and 3 MHz, 15 $V_{pp}$ at the second DEP electrode pair. Flow rate was 33 μl $h^{-1}$. (a) Initially all cells are seen randomly distributed within the droplet. (b) *Salmonella* cells were attracted to the DEP electrodes that are tilted upwards due to the pDEP force, and eventually accumulated to the upper half of the droplet as the droplet reached the end of the first DEP electrode pair. (c-d) The macrophage experiencing nDEP force gradually migrated towards the bottom side of the droplet as the downward-tilted electrode position became lower within the droplet. Most *Salmonella* cells still remained within the upper half of the droplet due to the internal circulation flow. (e-f) After droplet splitting, the daughter droplet #2 contained most of the *Salmonella* cells, while the daughter droplet #1 contained the macrophage and few *Salmonella* cells that were not completely separated.

To characterize the in-droplet separation efficiency between macrophage and *Salmonella*, a mixture of *Salmonella* cells and macrophages was encapsulated into droplets. After droplet generation containing this cell mixture (*Salmonella* cells vs. macrophage = 10 to 1 ratio), a macrophage and *Salmonella* cells can be seen randomly distributed within the droplets (Fig. 4(a)). As the droplets traveled through the first pair of DEP electrodes, *Salmonella* cells receiving pDEP force were attracted towards the electrode and accumulated along the tilted electrode, gradually moving to the upper half of the droplet, while the macrophage experiencing no DEP force remained randomly distributed (Fig. 4(b)). As the droplets traveled through the second pair of DEP electrodes, the cluster of *Salmonella* cells were released but remained circulating within the upper half of the droplet driven by the internal circulation flow force, while the macrophages receiving nDEP force gradually migrated to the lower portion of the droplet (Fig. 4(c-d)). At the droplet splitting region, majority of the *Salmonella* cells were separated into the daughter droplet #2, while the macrophages were separated into the daughter droplet #1 (Fig. 4(e-f)). When comparing the resulting daughter droplets, most of the host cells were successfully collected in the lower chamber, while most of the bacterial cells were successfully collected in the upper chamber, proving that the developed separation method can indeed be used in such cell mixture applications (Fig. S3(e-f)). Under the DEP

voltage of 15 $V_{pp}$ / 8 $V_{pp}$ and flow rate of 33 µl $h^{-1}$, 74 ± 8% of macrophages were successfully separated into the daughter droplet #1 (lower droplets), while 84 ± 5% of *Salmonella* cells were successfully separated into the daughter droplet #2 (upper droplets) (ESI videos #3 and #4).

## Discussion

The developed in-droplet cell separation system enables the manipulation and separation of two different cell types within a droplet by utilizing their different DEP responses at different applied DEP frequencies. The proposed in-droplet cell manipulation platform was characterized using a bacterial-host cell interaction model with macrophage (representing mammalian host cell) and *Salmonella* cell (representing pathogenic bacterial cell). When encapsulated individually within droplets, macrophages and *Salmonella* cells were separated into daughter droplets #1 and #2 at 100% and 98% efficiency, respectively. However, when the two cell types were mixed, 74% of macrophages and 84% of *Salmonella* cells were successfully collected into the corresponding daughter droplets. This drop in separation efficiency is due to the fact that as macrophages move from the top portion of the droplet to the lower portion of the droplet, it was observed that these macrophages physically knock out some *Salmonella* cells accumulated along the DEP electrode, as well as some of these *Salmonella* cells hider the clean movement of macrophages to the lower part of the droplet.

Compared to our previous work of DEP-based in-droplet cell concentration,[30] there are several advancements, both from technological perspective as well as from application perspective. In continuous-flow microfluidics, cell separation using a single DEP electrode (either pDEP or nDEP) is possible since cells can be selectively trapped or separated based on their flow trajectory differences. This is not possible in droplet format due to the internal circulation flow, thus the use of a single DEP electrode and single polarity DEP force as shown previously[30] cannot achieve in-droplet separation. In this work, both pDEP and nDEP were utilized using an up-sloped and down-sloped electrodes to manipulate each cell type in a sequential manner, overcoming the complications streaming from the internal recirculation flow. From application perspective, this novel design resulted in the first demonstration of in-droplet cell separation, whereas our prior work demonstrated in-droplet cell concentration, essentially a centrifugation step in droplet format. Other technologies, such as BAW or SAW, have demonstrated in-droplet cell manipulation, but no cell separation. There are many biological applications where in-droplet cell separation is needed, such as for host-pathogen interaction studies or drug screening applications. Overall, the new droplet application demonstrated here can benefit broad ranges of biological studies and enable more applications to be realized in droplet-based microfluidics platform.

In general, low conductivity media is used in order to manipulate particles or cells in DEP-based microfluidic systems. Since the magnitude of DEP force is proportional to the difference of dielectric properties between a cell and the surrounding solution, very weak DEP force is generated if cells are suspended in a normal culture media or Phosphate Buffered Saline (PBS) due to their similar dielectric properties with cells. To ensure that the use of low-conductivity medium do not affect the viability as well as functionality of cells, off-chip verification experiments were conducted using PBS as control. The result showed that more than 85% of the cells were viable over four hours of culture, which is in line with many other previous reports on DEP-based microfluidic system.[30-32, 34] Considering that generally 1 to 3 h are required for most cell-cell interaction assays depending on multiplicity of infection (MOI),[36, 37] we concluded that the use of low-conductivity media does not pose a great challenge to the viability of cells during the entire assay. In addition, we have conducted a cellular pathogenicity assay (adherence of bacterial cells to host cells) with cells in low-conductivity medium, and no differences were observed. Nevertheless, the fact that low conductivity solution is essentially needed in this DEP-based cell manipulation method is indeed a limitation in DEP-based cell manipulation applications.

After droplet splitting, the daughter droplets were collected and employed to examine cell viability (further details are described in the Experimental section). In-droplet *Salmonella* cells concentration was carried out under the conditions of 33 µl $h^{-1}$ at 15 $V_{pp}$, and the collected daughter droplets #2 were used for the viability test with live/dead staining. The result showed that 93 ± 0.5% of the cells after DEP manipulation were viable, compared to 94 ± 2% viability before DEP manipulation. Next, the viability of macrophages was analyzed after in-droplet macrophage manipulation under the conditions of 33 µl $h^{-1}$ at 8 $V_{pp}$. The daughter droplets #1 were collected and the viability was conducted with Evans blue staining. Compared to 95 ± 1% viability before DEP manipulation, 90 ± 3% of the cells were viable after DEP manipulation. Thus, it is clearly demonstrated that the cell viability was not drastically influenced by the applied voltage and the DEP force.

The sorting efficiency is sensitive to the channel height due to the planar DEP electrode layout. Only cells that are close to the bottom side of the droplet are relatively close to the DEP electrode and will experience the maximum DEP force, which suggests that the channel height has to be carefully determined to ensure that the generated electric field can have good coverage over the entire z-axis of the microfluidic channel. The x-directional electric field across the cell manipulation microchannel was simulated under different channel height conditions (Fig. S4). The average electric field intensity at the ceiling of the channel was 2.6, 2.2, and 1.8 ($\times 10^5$ V $m^{-1}$) where the channel height was 22, 26, and 30 µm, respectively. With only 4 µm difference in channel height, the electric field intensity drops by about 20% under the same voltage condition, which can decrease the separation efficiency. To minimize the impact stemming from the channel height, mirrored DEP electrode pairs could be potentially patterned on the ceiling side of the channel, creating a top-bottom electrode design. Fig. S4(d) shows the electric field

distribution in the case of a top-bottom electrode pair design so that the applied electric field can be intensified and be more uniform throughout the z-direction of the microfluidic channel.

In order to compare the forces acting on in-droplet bacterial and mammalian cells while a droplet passing through the cell concentration regions, COMSOL simulations (COMSOL Multiphysics® 5.5) of internal circulation flow field as well as electric field were performed (further details in supplementary document). The flow inside a droplet (seen in the middle x-z plane) shows uniform axisymmetric circulation pattern (Fig. S5). In addition, the capillary number, Ca, is $0.7\times10^{-3}$ under the given conditions used here, indicates that cells within a droplet would exhibit random distribution,[20] which is coherent to our observation (without DEP in ESI videos #1 and #2). The Stokes drag force was calculated based on average inertial circulation flow velocity obtained by the COMSOL simulation results. The $x$-directional DEP force for each cell type was calculated at the middle z plane (z = 13um) based on the simulation result of non-uniform electric field. Based on this calculation, the DEP force on bacterial cells (Fig. S6(a)) increases as bacterial cells become closer towards the edge of the electrode. Compared to the received Stokes drag force (12 pN), the pDEP force acting on bacterial cells can be as high as 39 pN when bacterial cells are right above the electrodes; therefore, pDEP force under this circumstance is high enough to overcome the Stokes drag force, enabling pDEP-based bacterial cell manipulation within a droplet. Similarly, the nDEP force (61 pN) acting on mammalian cell was greater than the Stokes drag force (61 pN), therefore can effectively repel cells from the electrodes. Additionally, we calculated that the Stokes drag force acting on mammalian cells reaches to 83 pN when the internal circulation flow field was simulated at total flow rate of 45 µl $h^{-1}$, which is larger than the calculated nDEP force for mammalian cell. Therefore, the Stokes drag force will dominate the trajectory of mammalian cells, where the DEP force in this case can no longer effectively manipulate these mammalian cells. These simulation and calculation results are indeed comparable to the experimental cell separation results under the three different flow rates (27, 33, and 39 µL $h^{-1}$), and may also explain the significant drop of mammalian cell separation efficiency that we observed at flow rate of 39 µL $h^{-1}$. Overall, these simulation and calculation can be utilized to select appropriate voltage, flow rate and channel dimension when applying the presented technology to other applications of interest.

The maximum voltage generated by a conventional low-cost function generator is up to 20 $V_{pp}$, so to apply a higher voltage that may be required for some applications, a voltage amplifier may be necessary. For example, in the case of bacterial cell separation as shown here, their size is relatively small compared to mammalian cells, requiring a higher voltage applied compared to only mammalian cell manipulation. An alternative method is to use 3D electrodes[38] embedded in the bottom substrate that can generate stronger electric field than that generated by the planar electrode under the same voltage condition, allowing the use a generic low-cost function generator.

The overall system throughput achieved so far in this work is 2 droplets per second. Increasing the flow rate to increase the throughput is a possibility, however, this leads to stronger internal circulation flow force (as we discussed above), meaning that a higher DEP voltage is required to achieve a similar separation efficiency. Considering the potential functional damage that higher voltage may bring to the more susceptible mammalian host cells, such approach is less preferred from biological perspective, but might be useful when handling more robust cells (such as bacterial cells). Alternatively, if a higher throughput is needed, a multi-channel parallel approach can readily achieve higher system-level throughput.

For further applications, DEP based separation is typically not possible when the *Clausius-Mossotti* factors of the two cells of interest are close to each other. However, cell size is also a main factor affecting DEP force. Thus, if the size of the two cell types are different enough, a well-optimized voltage condition should be able to manipulate only one target cell type with DEP force, which can then be separated from the mixture using a subsequent droplet splitting structure. Since there is no DEP force acting on undesired cells, they will be randomly distributed in the droplet and thus not fully discarded even after separation. In this case, removal efficiency is decided by the ratio of the width of Y-shaped splitting channels. In the device shown here, the width of each splitting channel is 130 and 70 µm, respectively, so ideally 65% of undesired cells where no DEP force is exerted on can still be removed. In such a scenario, the lower channel width can be adjusted depending on the application to maximize the separation efficiency.

Since DEP-based systems can be readily integrated into most microfluidic devices, the use of DEP for in-droplet cell manipulation opens up large number of possible applications where this system can be integrated into. These include integrating impedance and optical analysis systems for in-droplet cell counting and hit discrimination, electric field-based or pneumatic-based droplet sorting systems, and droplet merging systems for realization of droplet solution exchange, which is to perform more systematic assays on a single chip, to name a few.

## Experimental section

### Device design and feature dimension

Microfluidic channels here were 200 µm wide and 26 µm high. For each electrode pair, the electrodes were parallel to each other, and tilted 0.05° with respect to the microfluidic channel. The width of each electrode was 15 µm and the gap between the electrodes was 10 µm. The first pair of DEP electrodes was tilted upwards, starting at the bottom side of the channel, to the point at the upper side where a 20 µm wide spacing was left without electrode coverage of the microfluidic channel. The second pair of electrodes starts 200 µm behind the first

electrode pair with a downward tilt. At the splitting region, the widths of the upper and lower microfluidic channels were 120 µm and 70 µm, respectively.

**Microfabrication**

Cr/Au (200/1000 Å) layers were deposited by E-beam evaporation on 0.7 mm of borosilicate glass substrates (Swiftglass, Co., Inc., NY). After photolithography patterning with AZ 5214 photoresist (AZ Electronic Material plc, NJ), the metal layers were etched. Finally, the photoresist was removed in AZ 400T stripper at 95°C for 5 min. The patterned master molds for PDMS replication were fabricated by SU-8™ photoresist (Microchem, Inc., MA) using conventional photolithography processes. A 26 µm height master mold was obtained by spin-coating SU-8™ 2025 at a speed of 2800 rpm, and was then coated with Tridecafluoro-1,1,2,2-Tetrahydrooctyl-1-Trichlorosilan (United Chemical Technologies, Inc., Bristol PA) to facilitate PDMS replication. Microfluidic channels were fabricated with PDMS (10:1 mixture, Sylgard 184, Dow Corning, Inc., MI) using conventional soft lithography techniques. PDMS and borosilicate substrates with Au patterning were aligned under a microscope using deionized water (DI water) as a lubricant layer and bonded right after 90 seconds of oxygen plasma treatment. The aligned device was placed on a hotplate at 95 °C for overnight baking to completely remove any vapor residues. Right before the experiment, the microfluidic channel was rinsed with precious metal surfactant (Acuden Inc., CA, USA), baked, followed by rinsing with filtered fresh Aquapel (Pittsburgh Glass Works, LLC., PA) to ensure the hydrophobicity of the microchannel.

**Preparation of conductivity media**

In order to have greater relative displacement of cells within droplets, low conductivity media made of 0.3 mM of monopotassium phosphate (1551139, Sigma-Aldrich, USA), 0.85 mM of dibasic potassium phosphate (1151128, Sigma-Aldrich, USA), and 280 mM of myo-Inositol (I5125, Sigma-Aldrich, USA) were added into DI water to make the base media.[30, 34] Potassium chloride (2.5 mM, P9333, Sigma-Aldrich, USA) was added into this base media to achieve a conductivity of 0.032 S $m^{-1}$.

**Cell preparation**

J774A.1 (ATCC TIB67) macrophages were thawed and grown in T75 culture flasks with Dulbecco's Modified Eagle Media (DMEM, D5648, Sigma-Aldrich, USA) containing 10% Fetal Bovine Serum (FBS, 16000044, Thermo Fisher Scientific, USA) in a 37°C, 5% $CO_2$ incubator. Prior to the experiment, cell culture media was removed, and macrophages were rinsed with low conductivity media by three times. Cell were then detached by cell scrapping, and the cell concentration was adjusted to $1.25 \times 10^6$ cells $ml^{-1}$, which results in about three macrophages encapsulated into each droplet (size: 130 µm diameter, volume: 1.15 nL). *Salmonella Typhimurium* (strain ATCC 14028S) engineered with a GFP plasmid (pCM 18) was inoculated on a trypticase soy agar plate containing 50 µg $ml^{-1}$ erythromycin, followed by incubation at 37°C overnight. The next day, single colonies were picked and cultured in LB 50 µg $ml^{-1}$ erythromycin broth in a shacking incubator at 37 °C for 8 h. The bacteria culture was centrifuged and rinsed with low conductivity media by three times before the experiment. For the initial in-droplet *Salmonella* manipulation experiment, the concentration of *Salmonella* culture was adjusted to an OD of 1.0 and then further diluted by 50 times to have around 20 *Salmonella* cells per microdroplet. For the final macrophage-*Salmonella* mixed sample separation experiment, the concentration of macrophages was diluted to $4.2 \times 10^5$ cells $ml^{-1}$, and the *Salmonella* culture with OD of 1.0 was diluted by 100 times to obtain around one macrophage and 10 *Salmonella* cells encapsulated in each droplet.

**In-droplet cell separation operation**

The droplet microfluidic system was characterized using *Salmonella* cell suspension, macrophage suspension, and macrophage/*Salmonella* cell mixture, respectively. The total flow rate was varied from 27, 33 to 39 µl $h^{-1}$ to find the optimal operating condition. For every test condition, the flow rate of carrier oil (Novec 7500, 2.5% Pico-Surf surfactant, 3200278, Dolomite, USA) was adjusted depending on the cell solution flow rate so that droplets having a diameter of 130 µm could be consistently generated. For *Salmonella*, the first DEP electrode pair signal was set to 3 MHz, 9, 12, and 15 $V_{pp}$, while the second DEP electrode pair signal was set to a constant 100 kHz, 8 $V_{pp}$. For macrophage, a constant sinusoidal signal of 3 MHz, 15 $V_{pp}$ was applied to the first DEP electrode pair, and 100 kHz, 6, 7 and 8 $V_{pp}$ were applied to the second DEP electrode pair. For the mixed cell experiment, droplets were generated using the flow-focusing structure at a speed of 30 µl $h^{-1}$ for the carrier oil and 3 µl $h^{-1}$ for the cell solution, and then pushed by 33 µl $h^{-1}$ of carrier oil into the DEP cell manipulation/separation region.

**Cell viability assay**

Cell viability for *Salmonella* cells was evaluated by calculating the percentage of dead cells in the population. SYTO 9 dye (ex/em 485/530 nm) was used to stain viable cells, while nonviable cells were stained with propidium iodide (PI) (ex/em 485/630 nm) (live/dead baclight bacterial viability kit, L7012, Invitrogen), both staining solutions were mixed 1:1 ratio before use. After droplet splitting, the daughter droplet #1 were collected from the lower side outlet and resuspended in 1 ml PBS solution. 6 µl of combined reagent mixture was added, followed by incubation for 15 min at room temperature. The fluorescence microscopic (Zeiss AXIO Observer 7) images, which were acquired before/after in-droplet cell separation experiment, were used for cell viability analysis. In the case of macrophages, Evans blue dye (E2129, Sigma Aldrich), which only stains nonviable cells, was used for cell viability evaluation. The daughter droplet #1 were collected from the lower side outlet and suspended in PBS solution. The collected cells were resuspended with 1 ml of 1%

(w/v) stock solution of Evans blue and incubated for 5 min at room temperature. The sample was loaded into a hemocytometer and cell viability was measured using an inverted microscope.

### Statistical analysis of separation efficiency

To analyze the separation efficiency, a high-speed camera (Phantom micro lab100, Vision Research, Inc.) was used to capture the trajectory of cell migration (60 frames per second (fps) for *Salmonella*, 200 fps for macrophage). The camera was set to image at the droplet splitting region, and cells within each daughter droplet were counted frame by frame before/after the droplet splitting to calculate the separation efficiency. For each case, approximately 100 images were analyzed. Additional statistic microscopic (Zeiss AXIO Observer 7) pictures of daughter droplets were obtained at downstream collection chambers for the purpose of verification.

## Associated content

### Supporting Information

ESI video #1: Video showing Salmonella separation into the upper channel; (mp4)
ESI video #2: Video showing macrophage separation into the lower channel; (mp4)
ESI video #3 and #4: Videos showing separation of *Salmonella* and macrophages into corresponding channel; (mp4)
Supplementary document: Microscopic pictures of generated cell-encapsulated droplets, simulation results of real part of cells' *Clausius-Mossotti* Factor, microscopic pictures of collection chambers, comparison of COMSOL simulation results of generated electric field for DEP manipulation in bottom-only or bottom-top electrode setting, and calculation of in-droplet forces acting on cells based on COMSOL simulation; (doc)

## Author contributions

S.-I. H. and A. H. designed the experiments. S.-I. H. and C. H. performed the experiments, run the simulation, and analyzed the data. S.-I. H, C. H., and A. H co-wrote the manuscript, especially, A. H. supervised the work and wrote the manuscript.

## Conflicts of interest

Part of the presented technology has been filed for US patent.

## Acknowledgements

This project was supported by the United States Defense Advanced Research Project Agency (DARPA) Cooperative Agreement #W911NF1920013.

## References

1. E. Brouzes, M. Medkova, N. Savenelli, D. Marran, M. Twardowski, J. B. Hutchison, J. M. Rothberg, D. R. Link, N. Perrimon and M. L. Samuels, *Proc. Natl. Acad. Sci. U.S.A.*, 2009, **106**, 14195-14200.
2. M. T. Guo, A. Rotem, J. A. Heymanab and D. A. Weitz, *Lab on a Chip*, 2012, **12**, 2146-2155.
3. S. Mashaghi, A. Abbaspourrad, D. A. Weitz and A. M. v. Oijen, *TrAC Trends in Analytical Chemistry*, 2016, **82**, 118-125.
4. J. S. Barea, J. Lee and D.-K. Kang, *Micromachines*, 2019, **10**, 412.
5. M.-T. Chen and R. Weiss, *Nat. Biotechnol.*, 2005, **23**, 1551-1555.
6. Z. Klement, *Nature*, 1963, **199**, 299-300.
7. B. A. Sanford, A. Shelokov and M. A. Ramsay, *J. Infect. Dis.*, 1978, **137**, 176-181.
8. R. J. Shattock and G. E. Griffin, *Res. Virol.*, 1994, **145**, 139-145.
9. R. Wang, R. Kobayashi and J. M. Bishop, 1996, **93**, 8425-8430.
10. M. Antia, T. Herricks and P. K. Rathod, *PLoS Pathogens*, 2007, **3**, e99.
11. Z. Wang, M.-C. Kim, M. Marquez and T. Thorsen, *Lab Chip*, 2007, **7**, 740.
12. T. Xu, W. Yue, C.-W. Li, X. Yao, G. Cai and M. Yang, *Lab Chip*, 2010, **10**, 2271.
13. T. Herricks, K. B. Seydel, G. Turner, M. Molyneux, R. Heyderman, T. Taylor and P. K. Rathod, *Lab Chip*, 2011, **11**, 2994.
14. J. Yang, Z. Chen, P. Ching, Q. Shi and X. Li, *Lab Chip*, 2013, **13**, 3373.
15. S. Katz, M. Izhar and D. Mirelman, *Ann. Surg.*, 1981, **194**, 35-41.
16. S. K. Ogawa, E. R. Yurberg, V. B. Hatcher, M. A. Levitt and F. D. Lowy, *Infect. Immun.*, 1985, **50**, 218-224.
17. E. C. Boyle and B. B. Finlay, *Curr. Opin. Cell Biol.*, 2003, **15**, 633-639.
18. G. K. Kurup and A. S. Basu, *Biomicrofluidics*, 2012, **6**, 022008.
19. M. Sun, Z. S. Khan and S. A. Vanapalli, *Lab Chip*, 2012, **12**, 5225.
20. M. Hein, M. Moskopp and R. Seemann, *Lab Chip*, 2015, **15**, 2879-2886.
21. D. Lombard and P. S. Dittrich, *Analytical and Bioanalytical Chemistry*, 2011, **399**, 347-352.
22. E. Brouzes, T. Kruse, R. Kimmerling and H. H. Strey, *Lab on a Chip*, 2015, **15**, 908-919.
23. R. Gao, Z. Cheng, A. J. deMelloc and J. Choo, *Lab on a Chip*, 2016, **16**, 1022-1029.
24. A. Fornell, J. Nilsson, L. Jonsson, P. K. Periyannan Rajeswari, H. N. Joensson and M. Tenje, *Anal. Chem.*, 2015, **87**, 10521-10526.
25. A. Fornell, M. Ohlin, F. Garofalo, J. Nilsson and M. Tenje, *Biomicrofluidics*, 2017, **11**, 031101.
26. A. Fornell, C. Johannesson, S. S. Searle, A. Happstadius, J. Nilsson and M. Tenje, *Biomicrofluidics*, 2019, **13**, 044101.
27. A. Fornell, K. Cushing, J. Nilsson and M. Tenje, *Appl. Phys. Lett.*, 2018, **112**, 063701.
28. K. Park, J. Park, J. H. Jung, G. Destgeer, H. Ahmed and H. J. Sung, *Biomicrofluidics*, 2017, **11**, 064112.
29. J. Park, G. Destgeer, H. Kim, Y. Cho and H. J. Sung, *Lab on a Chip*, 2018, **18**, 2936-2945.

30. S.-I. Han, H. S. Kim and A. Han, *Biosensors and Bioelectronics*, 2017, **97**, 41-45.
31. K.-H. Han, S.-I. Han and A. B. Frazier, *Lab Chip*, 2009, **9**, 2958.
32. S.-I. Han, S.-M. Lee, Y.-D. Joo and K.-H. Han, *Lab on a Chip*, 2011, **11**, 3864-3872.
33. T. Z. Jubery, S. K. Srivastava and P. Dutta, *ELECTROPHORESIS*, 2014, **35**, 691-713.
34. S.-I. Han, H. S. Kim, K.-H. Han and A. Han, *Lab Chip*, 2019, **19**, 4128-4138.
35. P. R. C. Gascoyne and J. V. Vykoukal, *Proc. IEEE*, 2004, **92**, 22-42.
36. J. M. Timpe, M. M. Holm, S. L. Vanlerberg, V. Basrur and E. R. Lafontaine, *Infect. Immun.*, 1991, **59**, 822-828.
37. J. M. Timpe, M. M. Holm, S. L. Vanlerberg, V. Basrur and E. R. Lafontaine, *Infaction and Immunity*, 2003, **71**, 4341-4350.
38. A. R. Guzman, H. S. Kim, P. De Figueiredo and A. Han, *Biomed. Microdevices*, 2015, **17**, 35.